Journal of The Electrochemical Society, **164** (14) A1-A9 (2017)
0013-4651/2017/164(14)/A1/9/$37.00 © The Electrochemical Society

Exploring Interactions between Electrodes in $Li[Ni_xMn_yCo_{1-xy}]O_2$/Graphite Cells through Electrode/Electrolyte Interfaces Analysis

Lénaïc Madec[a,c,d,z] and Leah D. Ellis[b,*]

[a]*Department of Physics and Atmospheric Science, Dalhousie University, Halifax, Nova Scotia B3H 4R2, Canada*
[b]*Department of Chemistry, Dalhousie University, Halifax, Nova Scotia B3H 4R2, Canada*

Interactions occurring between positive and negative electrodes during constant current-constant voltage cycling in $Li[Ni_xMn_yCo_{1-xy}]O_2$/graphite pouch cells at various upper cutoff voltages was investigated. Below 4.3 V, good capacity retention, high/stable coulombic efficiency (CE) and low gas production were observed. At 4.5 V, however, extensive capacity loss, dramatic/unstable CE and large gas generation were observed due to extensive electrolyte degradation at the NMC electrodes. XPS experiments highlighted that solvents (-CO containing species) and salt (mostly LiF) degradation products including gas and NMC dissolution products are produced at the NMC electrodes then migrate to the graphite electrodes surface where they are either reduced or simply deposited. Although these phenomena were greatly accelerated at high voltage, the dominant failure mechanism was the formation of a Li-ion insulator/electron conductor surface layer (maybe rock salt) due to irreversible structural change of the NMC particles surface. At low voltage, the failure mechanism was explained by accumulation of SEI at the graphite electrode surface that hinder the ionic transport through the electrode porosity. Overall, both failure mechanisms are driven by oxidative parasitic reactions at the positive electrode and interaction with the negative electrode. Passivation of the positive electrode appears therefore crucial to promote long lifetime of Li-ion cells.

Manuscript submitted November 14, 2017; revised manuscript received November 27, 2017. Published 00 0, 2017.

High energy density Li-ion cells can in theory be made if positive electrode materials such as $Li[Ni_xMn_yCo_{1-xy}]O_2$ (NMC) operate to 4.7 V.[1] Severe electrolyte degradation occurs, however, at the positive electrolyte/electrode interfaces above 4.3 V vs. Li/Li^+ which leads to large cell impedance and short lifetime[2–4] thus greatly limiting the practical use of such material at high voltage. To overcome this limitation, electrolyte additives are widely used as they offer so far the most simple, economical and effective approach.[5,6] Electrolyte additives are well known to modify and stabilize the Solid Electrolyte Interphase (SEI)[7] therefore hindering unwanted parasitic reactions. Among electrolyte additives, vinylene carbonate (VC)[8] is likely the most used as it allows significant improvements of cycle/calendar life and thermal stability of numerous Li-ion systems.[9–15] The main drawback remains, however, the extensive electrolyte degradation occuring for VC-containing cells at high potentials[16] and high temperatures[17] that leads to capacity losses, impedance rise and gas evolution. To bypass this issue, sulfur-containing additives have been recently proposed to enable the use of high voltage Li-ion cells. So far, methylene methane disulfonate (MMDS)[18–24] and prop-1-ene-1,3-sultone (PES)[25–30] are probably the most promising ones. For instance, PES produced significantly lower gas during long term cycling and storage at 60°C compared to identical cells containing VC.[28–30] These results can be explained by the formation of more protective and stable SEI films at both graphite and positive electrode surfaces as observed by XPS experiments,[27,28,31] due to the preferential reaction of PES at both electrode surfaces.[32]

More generally, the effect of the electrolyte composition as function of various upper cutoff voltages and Li-ion cell chemistries is increasingly investigated. For instance, some studies focused on the impact of the upper cutoff voltage on the electrochemical performance[4,33,34] with interestingly a recent growing use of aggressive constant courant-constant voltage (CC-CV) cycling.[35,36] Also, fundamental studies on the electrode/electrolyte interfaces using surface analysis by X-ray photoelectron spectroscopy (XPS) are now widespread even after storage[37] and long term cycling.[38,39] In particular, phosphorus enrichment of SEI films have been observed for various high voltage materials using $LiPF_6$-based electrolytes, highlighting a Li-salt decomposition as function of the voltage[40] which recently motivated the use of $LiPF_6$ hydrolysis products as electrolyte additives to stabilize the positive electrode at high voltage.[41] Recently, the use of electrochemical impedance spectroscopy (EIS) on symmetric cells has received great interests as it allows to distinguished from which electrode the impedance grow arises during cycling.[42,43] For instance, EIS on symmetric cells extracted from NMC442/graphite pouch cells showed that the impedance growth above 4.4 V was dominated by contributions from the NMC442 electrode while the contribution of the graphite electrode does not depend on the upper cutoff voltage.[34] Similarly, three-electrode impedance spectroscopy also showed that the impedance growth during cycling of automotive $LiNi_{0.8}Co_{0.15}Al_{0.05}O_2$/graphite battery originated from rising R_{ct} and R_{SEI} at the positive electrode.[44] Theoretical simulation of EIS spectra further confirmed that experimental high voltage impedance growth is primarily due to increases in charge transfer and SEI resistances at the positive electrode.[45] Recent transmission electron microscopy (TEM) studies pointed out that structural change (rock salt formation) of the $LiNi_{0.8}Co_{0.15}Al_{0.05}O_2$ and $Li[Ni_xMn_yCo_{1-xy}]O_2$ material surface upon cycling is more likely the main cause of the impedance growth at the electrode/electrolyte interface at high voltage as well as the first-cycle coulombic inefficiency.[46–48] This hypothesis is supported by a recent report of Buchberger et al.[49] that showed using XRD analysis that the lithium content in $Li_xNi_{1/3}Mn_{1/3}Co_{1/3}O_2$ is about 0.8 after 230 cycles at 4.6 V stopped in discharge while the capacity retention is about 35% which means that the NMC electrode contains unused cyclable lithium and that the total capacity loss is mainly due to kinetic limitation rather than a Li inventory loss. Nelson et al.[34] also confirmed this kinetic limitation phenomena as after 80 CC-CV cycles at various high voltages, NMC/graphite pouch cells could deliver discharge capacities very close to their initial ones when sufficiently slow cycling (C/50) was selected.

Moreover, the stability of the inactive component of positive electrodes such as conductive carbons have recently been proved to participate in the electrolyte degradation at high voltage[50,51] using GC-MS analysis for instance.[52–54] Despite such plethora of studies, interactions between positive and negative electrodes that occur through diffusion of electrolyte degradation products are, however, not well identified while observed by different groups[55–58]. Therefore, still little is known about positive-negative interaction while they might be critical to a certain extent to the formation and growing of the SEI films at both electrodes, thus critical to the resulting lifetime of Li-ion cells. The

*Electrochemical Society Student Member.
[c]Present address: Université de Pau et des Pays de l'Adour, CNRS UMR 5254, IPREM, 64053 Pau, France.
[d]Present address: Réseau sur le Stockage Electrochimique de l'Energie (RS2E), CNRS FR3459, 80039 Amiens Cedex, France.
[z]E-mail: lenaic.madec@univ-pau.fr

most known interaction is the dissolution of positive active materials at high voltage that results in the deposition of metal-based species at the negative electrodes surface.[59,60] Recently, Metzger et al.[61] studied possible interactions between electrodes using a two-compartment cell connected to on-line electrochemical mass spectrometry (OEMS). Positive and negative electrodes were either not separated or separated by a Li^+-ion Al-sealed conducting glass blocking any other diffusion. They showed that in NMC/graphite cells, the generation of H_2 was drastically increased at high voltage and high temperature due to diffusion of protic electrolyte oxidation species ($R\text{-}H^+$) from the NMC to the graphite electrodes where they were reduced to H_2. Xiong et al.[62] showed that H_2 was generated during storage at 60°C in charged NMC/graphite pouch cells at high voltage while it was not for pouch bag containing either the lithiated graphite or the delithiated NMC electrode plus the electrolyte highlighting again that H_2 results from species created at the NMC electrode that diffuse to the graphite electrode to be reduced to H_2. Moreover, they showed that during storage at 60°C, charged NMC/graphite pouch cells at high voltage produced small amount of gas while for the pouch bag containing either lithiated graphite or delithiated NMC electrodes plus electrolyte, no gas and large amount of gas were produced, respectively[62,63]. This phenomena was associated with a large impedance increase of the NMC electrodes from the pouch bags compared to the NMC electrodes from the pouch cell which further confirms the occurrence of interactions between electrodes for the full cell with the gas produced at the NMC electrodes reduced at the graphite electrodes. Interestingly, using EIS on symmetric cells and XPS analysis, Petibon et al.[64] showed that even in NMC/graphite held at only 3.9 V or 4.2 V, the graphite electrodes surface drastically changed despite that only the NMC electrode potential changed. Again, this phenomena was attributed to diffusion of oxidative products from the NMC to the graphite electrodes.

The aim of this work is to investigate interactions occurring between positive and negative electrodes upon cycling in NMC/graphite pouch cells operating at different upper cutoff voltages. To do so, we used $Li[Ni_{1/3}Mn_{1/3}Co_{1/3}]O_2$ (NMC111)/graphite and $Li[Ni_{0.42}Mn_{0.42}Co_{0.16}]O_2$ (NMC442)/graphite pouch cells balanced for 4.2 or 4.7 V and 4.5 and 4.7 V operation, respectively. For each batch of NMC pouch cells, two different cutoff voltages were selected so that only the potential of the NMC electrodes was changed while the potential of the graphite electrodes remained constant (on the last plateau) as validated using a differential potential analysis software previously developed at Dalhousie University[6,5] PES was selected as electrolyte additive based on our previous detailed electrochemical[29,30], XPS[31,66], GC-MS[31,64,67] and theoretical[32] analysis. Aggressive CC-CV cycling at 40°C was used to accelerate the ageing of the cells. EIS experiments and gas volume were measured upon cycling to follow the impact of degradation phenomena upon the CC-CV cycling. The resulted electrode/electrolyte interphases were investigated by thorough XPS analysis of the SEI films formed at both NMC and graphite electrodes surface after the CC-CV cycling at different upper cutoff voltages.

Experimental

Cell preparation.—Machine made 240 mAh $LiNi_{1/3}Mn_{1/3}Co_{1/3}O_2$/graphite pouch cells balanced for 4.2 V (NMC111-4.2) or 4.7 V (NMC111-4.7) as well as 240 mAh $LiNi_{0.42}Mn_{0.42}Co_{0.16}O_2$/graphite pouch cells balanced for 4.5 V (NMC442-4.5) or 4.7 V (NMC442-4.7) were obtained dry (vacuum-sealed with no electrolyte) from Li-Fun Technology (Xinma Industry Zone, Golden Dragon Road, Tianyuan District, Zhuzhou City, Hunan Province, PRC, 412000). The electrolyte was 1 M $LiPF_6$ (BASF, purity 99.94, water content <20 ppm) in EC:EMC (3:7 by weight, BASF, water content <20 ppm) to which 2 wt% PES (Lianchuang Medicinal Chemistry Co., 98.2%) was added. After heating to 80°C under vacuum for 12 h to remove residual water, the pouch cells were filled with 0.9 g of electrolyte in an argon-filled glove box then vacuum-sealed at −94 kPa (relative to atmospheric pressure) using a compact vacuum sealer (MSK-115A, MTI Corp.). For each of the following electrochemical experiments, two identical pouch cells were prepared for reproducibility.

Cell formation and cycling protocols.—Cells were formed and cycled using a Maccor 4000 series battery cycler and a home-made temperature-controlled box at 40. ± 0.1°C.

Formation.—Cells were first held at 1.5 V for 24 h (for completion of wetting) then charged to 3.8 V at C/20. Cells were then cut open in an argon-filled glove box to release any gas generated and vacuum sealed again. Cells were then charged at C/20 either to 4.2 V (NMC111-4.2) or 4.5 V (NMC111-4.7, NMC442-4.5 and NMC442-4.7) and the degassing procedure was repeated except for NMC111-4.2. Cells were then partially discharged to 3.8 V at C/20 where impedance spectra were measured followed by a complete discharge to 2.8 V at C/20. An additional cycle was then performed at C/20 as follow. NMC111-4.2 cells were charged to either 3.9 V or 4.2 V while NMC111-4.7, NMC442-4.5 and NMC442-4.7 cells were charged to either 4.3 V or 4.5 V. Then, all cells were discharged to 2.8 V.

Constant current-constant voltage cycling (CC-CV).—One cycle of charge-hold-discharge protocol consisted of a constant current charge at C/5 to 3.9 or 4.2 V for NMC111-4.2 cells and to 4.3 or 4.5 V for NMC111-4.7, NMC442-4.5 and NMC442-4.7 cells, followed by a constant voltage step at the top of charge for 24 h, then a constant current discharge to 2.8 V at C/5. Additionally, every 10 cycles, cells underwent a slow C/20 constant current cycle during which the impedance spectra were measured at 3.8 V during charge. Before to be used for XPS analysis, all cells were held at 2.8 V at the end of the last discharge at C/20 until the measured current decreased to 0.005C so that electrodes were in electrochemical equilibrium.

Electrochemical impedance spectroscopy (EIS) measurements.—To measure the impedance spectra at 3.8 V during formation and cycling, cells were moved to a 10. ± 0.1°C temperature box. Impedance spectra were then collected using a Biologic VMP-3 with ten points per decade from 100 kHz to 10 mHz and a signal amplitude of 10 mV.

Gas measurements.—Gas evolution measurements based on Archimedes' principle were performed before and after each formation step as well as after the charge-hold-discharge (CC-CV) cycling by weighing cells submerged in de-ionized nanopure water (18 M) at 20 ± 1°C as described elswhere.[68]

X-ray Photoelectron spectroscopy (XPS).—*Sample preparation.*—At the end of the CC-CV cycling procedure (i.e. 30 CC-CV cycles) at 2.8 V after discharge, pouch cells were disassembled in an argon-filled glove box within the first 12 h following the end of the electrochemical process. Graphite and NMC electrodes were cut from the pouch cell electrodes with a precision punch and washed twice by immersion into 0.8 mL of EMC solvent (BASF) in a clean and dry glass vial with a mild manual agitation for 10 s to remove the $LiPF_6$ salt. Air sensitive samples were then mounted onto a molybdenum holder using a copper conductive tape (3M) under argon and placed into a special transfer system.[69] The latter was then put under vacuum at approx. 10^{-3} mbar for 1 h and then connected to the spectrometer where samples were loaded under a pressure of $\sim 10^{-3}$ mbar. All samples were kept at 10^{-8} mbar for one night before analysis to ensure a strictly identical vacuum procedure.

Data acquisition and treatment.—XPS was performed on a SPECS spectrometer equipped with a Phoibos 150 hemispherical energy analyzer and using Mg Kα radiation ($h\nu = 1253.6$ eV). The analyzed sample area was $\sim 2 \times 3$ mm^2 which gave results representative of the whole electrode. Core spectra were recorded in the fixed analyser transmission (FAT) mode with pass energy of 20 eV at an operating pressure $< 2 \times 10^{-9}$ mbar. First, short acquisition time spectra

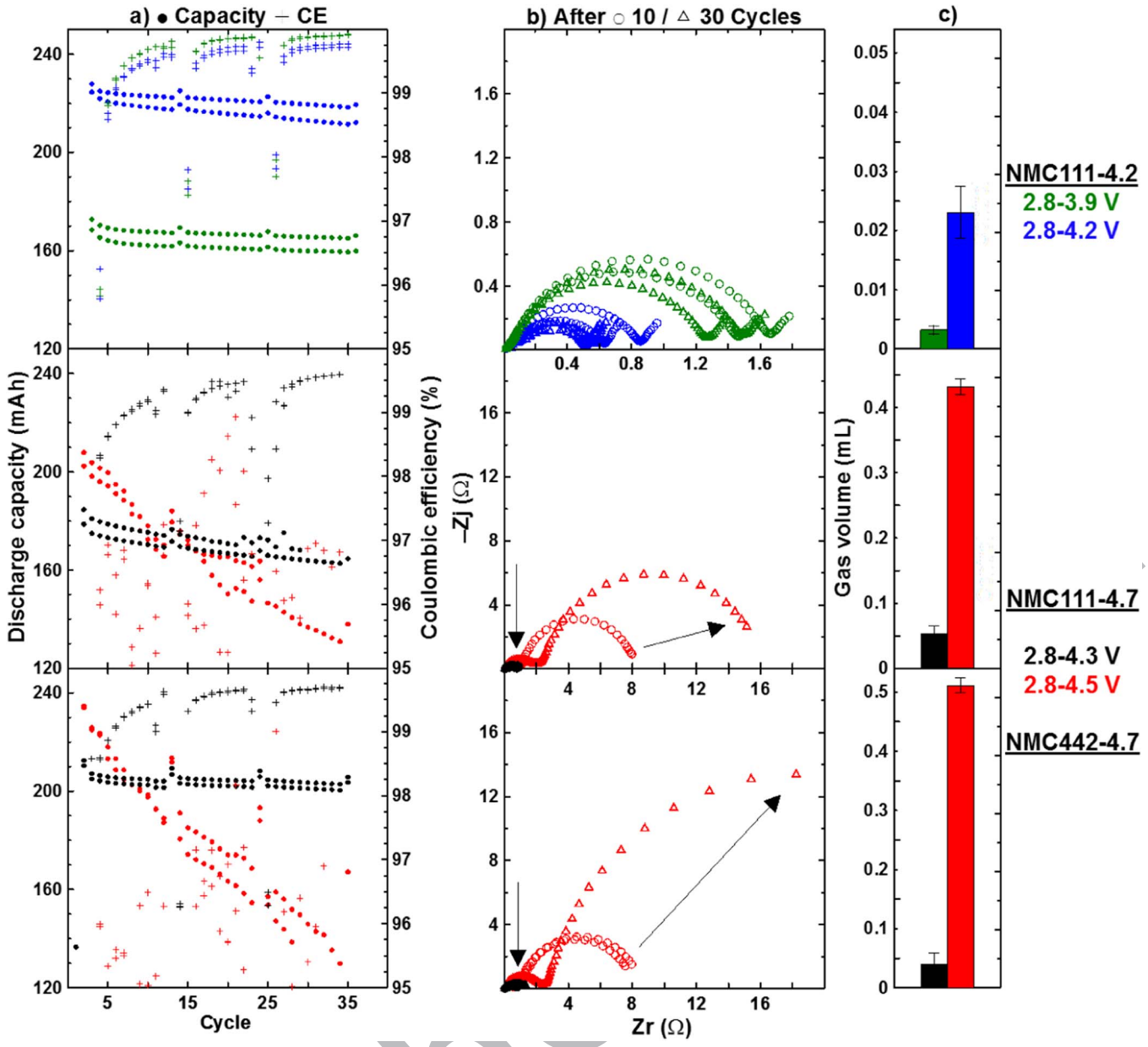

Figure 1. a) Discharge capacity and coulombic efficiency as function of cycle number, b) Nyquist plots after 10 and 30 cycles as well as c) volume of gas formed after 30 cycles for NMC111–4.2, NMC111-4.7 and NMC442-4.7 pouch cells with 2% PES electrolyte that underwent the charge-hold-discharge (CC-CV, C/5 CC-24h CV) cycling at 40. ± 0.1°C between 2.8 and various upper cutoff voltages as indicated. Note that the scales for impedance spectra and gas volume change as soon as pouch cells underwent the CC-CV procedure between 2.8 and 4.5 V.

were recorded as references to follow any possible degradation upon analysis. Data treatment was performed using CasaXPS software and the binding energy scale was calibrated from the C1s peak at 285 eV (C-C/C-H) and the O1s peak at 529.6 eV (O^{2-} anion from the NMC) for the graphite and NMC electrodes, respectively. A nonlinear Shirley-type background[70] was used for core peaks analysis while 70% Gaussian - 30% Lorentzian Voigt peak shapes and full width at half-maximum (FWHM) constraint ranges were selected to optimize areas and peak positions.

Results and Discussion

Long term cycling, impedance and gas analysis.—Figure 1a shows the discharge capacity and coulombic efficiency (CE) as function of cycle number for the NMC111-4.2, NMC111-4.7 and NMC442-4.7 pouch cells with 2% PES electrolyte that underwent the charge-hold-discharge (CC-CV, C/5 CC-24h CV) cycling at 40. ± 0.1°C between 2.8 and various upper cutoff voltages as indicated. Considering the severe CC-CV cycling, NMC/graphite pouch cells showed good capacity retention up to 4.3 V except for NMC111 balanced for 4.7 V. NMC/graphite pouch cells cycled at 4.5 V showed, however, extensive capacity losses. These results are associated to high and stable CE up to 4.3 V and dramatic and unstable CEs at 4.5 V. Note that after the C/20 cycle performed every 10 CC-CV, all cells showed a CE drop followed by an increase. This is more likely due to the dynamics behavior of the SEI and would need dedicated studies to be fully understood. Figure 1b shows the evolution of the Nyquist plots for the same NMC/graphite pouch cells between 10 and 30 CC-CV cycles. NMC/graphite pouch cells cycled up to 4.3 V showed very stable impedances. When cycled at 4.5 V, however, large impedance increases were observed as highlighted by the significant scales change. Figure 1c shows the volume of gas formed in the same

NMC/graphite pouch cells after the CC-CV cycling. For reference, the initial volumes of the pouch cells is 2.2 mL. NMC/graphite pouch cells cycled up to 4.3 V produced relatively low amount of gas (<0.05 mL). When cycled at 4.5 V, however, large volume of gas (0.2–0.5 mL) were generated. This is explained by extensive electrolyte degradation occurring at the NMC electrodes as soon as the cells are exposed for too much time at potentials above 4.3 V, in good agreement with the low coulombic efficiency observed at 4.5 V (Figure 1).

As a whole, it is believed that NMC/graphite pouch cells cycled at 4.5 V form either unstable or inefficient (i.e. not passivating) SEI layers at the NMC electrodes surface resulting in extensive electrolyte degradation that agrees well with the low CE and large volume of gas observed. Moreover, considering that the SEI films formed at the NMC electrodes surface cannot hinder severe parasitic reactions to occur at 4.5 V, an increase of the SEI resistance is thus unlikely. Therefore, charge transfer resistance increase at the NMC particles surface at 4.5 V is considered as the main cause for the large impedance rises and the resulting extensive capacity losses observed, in agreement with previous reports.[34,44,45,71] Accordingly, despite that the severe electrolyte degradation observed at 4.5 V probably results in Li inventory loss, this phenomena has certainly a limited effect on the total capacity losses. Indeed, when similar NMC/graphite pouch cells underwent a sufficiently slow cycling (C/50) after 80 CC-CV cycles at 4.4, 4.45 or 4.5 V, discharge capacities very close to their first cycle ones were observed.[34] Finally, the origin of the charge transfer resistance increase at 4.5 V can be explained by irreversible structural change of the NMC particles surface upon cycling similarly to previous observations.[46–48] Such new surface layer would therefore be inactive toward Li intercalation but its formation/properties would remain ineffective toward electrolyte degradation.

XPS analysis.—The effects of the upper cutoff voltage on both the graphite and NMC electrode/electrolyte interfaces was then investigated by XPS after the CC-CV cycling procedure (i.e. 30 CC-CV cycles) at 2.8 V after discharge. In the following Figures, core level spectra for a given element were normalized to show the relative intensity/amount of the given element between samples. To do so, the following procedure was used: considering that for a given peak, its FWHM was very close (<0.1 eV) from one sample to another, it is therefore possible to use the height (i.e. intensity) of the given peak to directly represent atomic percentage from one sample to another. Then, for each elements, the sample having the given peak with the highest atomic percentage was maximized in the Figure. Finally, core level spectra for other samples were normalized relatively.

At this point, it is important to clarify the following: considering that XPS analysis was performed after strictly identical cycle number, one may want to explain any difference observed in XPS between low and high voltages by a longer cycling time. However, NMC111-4.2 cells cycled about 10% more time at 4.2 V compared to 3.9 V, NMC111-4.7 cycled similar time and NMC442-4.7 cycled about 10% less time at 4.5 V compared to 4.3 V. This is due to the large impedance (i.e. polarization) increase observed at 4.5 V that led to lower capacity retention and concomitant lower cycling time (Figure 1). Therefore, any difference observed in XPS for the three sets of NMC/graphite cells between low and high voltages can only be explained by a voltage dependence.

Carbon 1s.—The Carbon 1s XPS core spectra of both graphite and NMC electrodes as taken from the different NMC/graphite pouch cells after the CC-CV cycling procedure (i.e. 30 CC-CV cycles) at 2.8 V after discharge are shown on Figures 2 and 3, respectively. Typical Carbon 1s XPS core spectra of fresh graphite and NMC electrodes are also showed for comparison. The C 1s spectrum of fresh graphite electrode showed five components at 284.1 (C=C), 286.9 (-CO), 288.6 ($-CO_2$), 290.8 eV (''shake up'' satellite) from the graphite and 285.0 eV (C-C/C-H) from the SBR binder[72] and graphite[73,74] (Figure 2). The C 1s spectrum of the fresh NMC electrode showed five peaks at 284.6

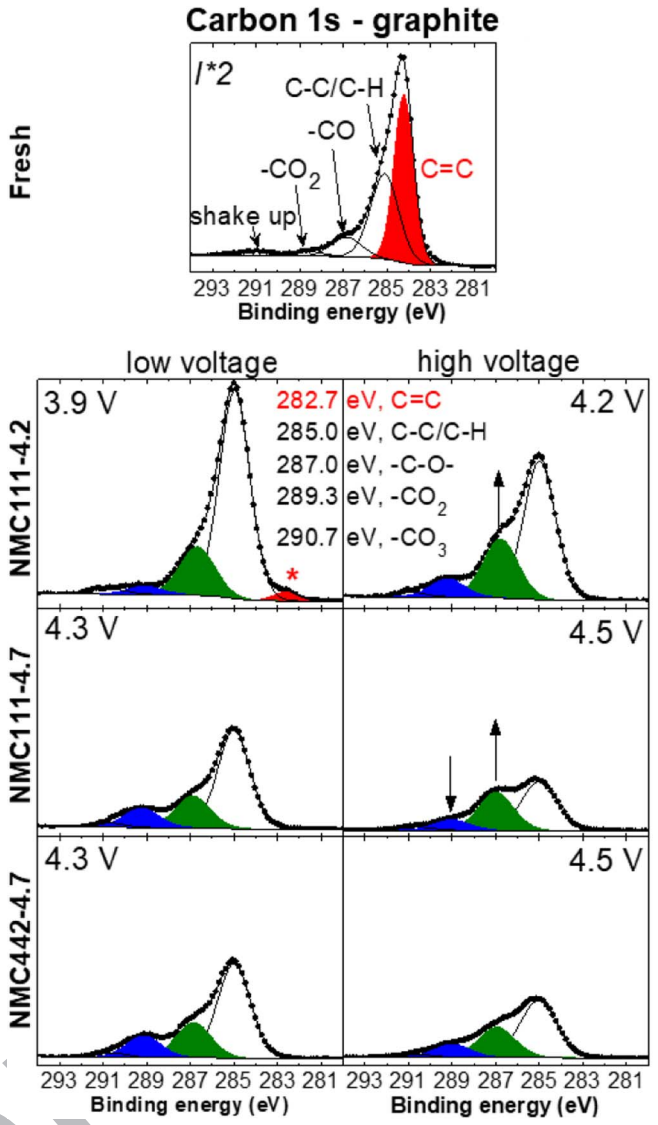

Figure 2. Carbon 1s XPS core spectra of graphite electrodes as taken from the different NMC/graphite pouch cells after the CC-CV cycling procedure (i.e. 30 CC-CV cycles) at 2.8 V after discharge. ~~Typical Carbon 1s XPS core spectra of fresh graphite and NMC electrodes are also showed for comparison.~~

(C=C), 286.9 (-CO), 288.9 eV ($-CO_2$) from the carbon black[73,74] and 285.9 (C-C/C-H), 290.7 eV from the PVdF binder (Figure 3).[72]

After the CC-CV cycling, no graphite peak was observed except for the cells cycled at 3.9 V (Figure 2). This indicates, in good agreement with the coulombic efficiencies (Figure 1a), that SEI films formed at the graphite electrodes surface are thinner than the 5–10 nm analyzed by XPS when cycled to 3.9 V and thicker than the 5–10 nm analyzed by XPS when cycled at higher voltages. A thin SEI film at 3.9 V is, however, unexpected considering the use of aggressive CC-CV cycling which emphasizes a very low rate of parasitic reactions at 3.9 V. The Carbon 1s XPS core spectra of the NMC electrodes (Figure 3) revealed that after the CC-CV cycling, the intensity of the carbon black peak at 284.6 eV slightly decreased for all pouch cells which means that relatively thin SEI films are formed at the carbon black surface of the positive electrodes upon cycling. Note that such phenomenon has never been reported until very recently[50–54] as carbon blacks were generally believed to be inert in positive electrodes. This phenomenon was, however, more pronounced as the cycling voltage increased indicating that thicker SEI films are formed at the carbon black surface, especially at 4.5 V.

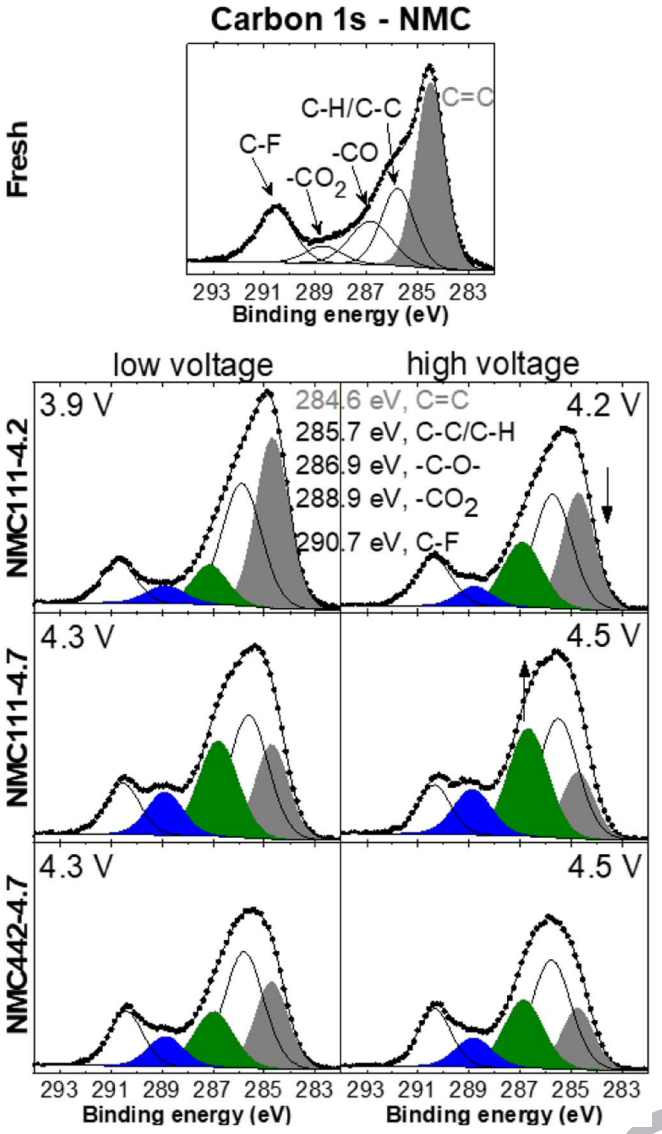

Figure 3. Carbon 1s XPS core spectra of NMC electrodes as taken from the different NMC/graphite pouch cells after the CC-CV cycling procedure (i.e. 30 CC-CV cycles) at 2.8 V after discharge. ~~Typical Carbon 1s XPS core spectra of fresh graphite and NMC electrodes are also showed for comparison.~~

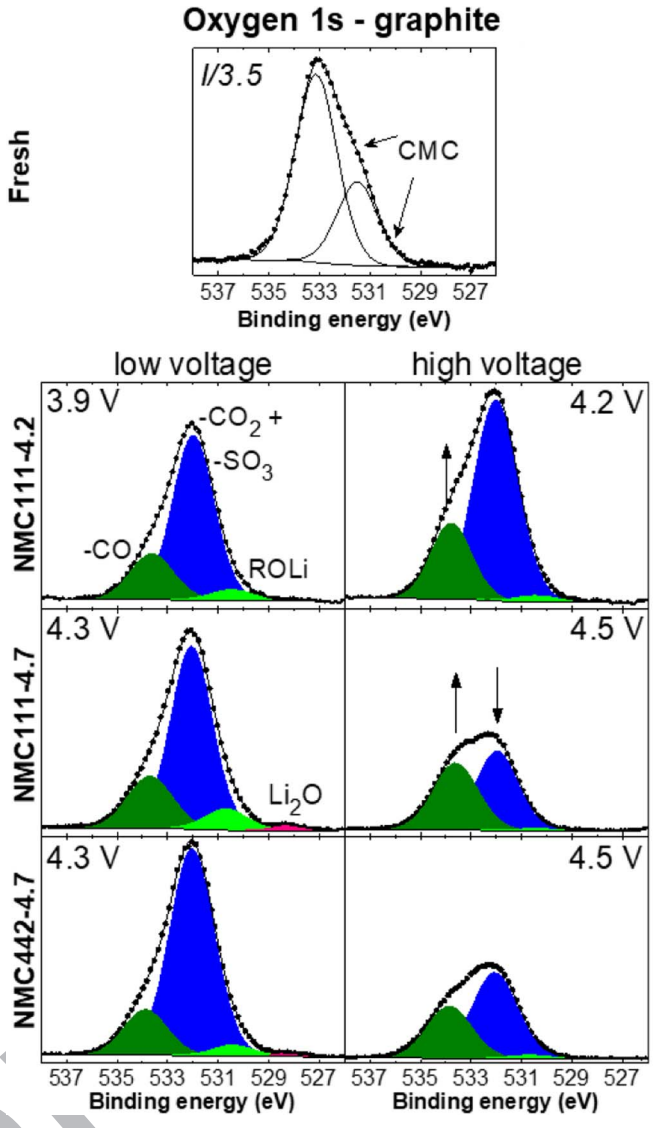

Figure 4. Oxygen 1s XPS core spectra of graphite electrodes as taken from the different NMC/graphite pouch cells after the CC-CV cycling procedure (i.e. 30 CC-CV cycles) at 2.8 V after discharge. ~~Typical Oxygen 1s XPS core spectra of fresh graphite and NMC electrodes are also showed for comparison.~~

Oxygen 1s.—The Oxygen 1s XPS core spectra of both graphite and NMC electrodes as taken from the different NMC/graphite pouch cells after the CC-CV cycling procedure (i.e. 30 CC-CV cycles) at 2.8 V after discharge are shown on Figures 4 and 5, respectively. Typical Oxygen 1s XPS core spectra of fresh graphite and NMC electrodes are also showed for comparison. The O 1s spectrum of the fresh graphite electrode showed two components at 531.6 and 533.4 eV from the CMC binder (Figure 4).[72] The O 1s spectrum of the fresh NMC electrode showed three peaks assigned to O^{2-} anions from the lattice oxygen of the NMC at 529.5 eV and oxygen anions with deficient coordination at the NMC surface[72] and/or -CO_x-like oxygen from the carbon black[73,74] (referred to as surface oxygens) (Figure 5).

After the CC-CV cycling, the intensity of the 529.5 eV peak from NMC decreased more significantly (Figure 5) compared to what was observed for the carbon black peak at 284.6 eV (Figure 3). This result means that SEI films formed at the NMC active material surface are more likely thicker than at the carbon black surface. While this result may originate from different catalytic electrolyte degradation effects at the NMC surface compared to the carbon black surface, possible exchange of SEI species between the active NMC particles and the carbon black have also to be considered.[75] More interestingly, between 3.9 V and 4.2 V, the intensity of the NMC peak at 529.5 eV was decreased while between 4.3 V and 4.5 V, the intensity of this peak increased. This result is thus unexpected if one consider that the higher electrolyte degradation observed at 4.5 V (Figure 1) should lead to higher degradation products deposited at the NMC electrodes surface. This suggests that the parasitic reactions occurring at 4.5 V lead to species that can migrate to the graphite electrode instead of being deposited at the NMC electrodes. Therefore, considering the large impedance increase observed after CC-CV cycling at 4.5 V (Figure 1b), it is believed that the oxidized species are generated together with electrons and that these electrons can somehow reacts at the NMC electrodes surface to form a new surface layer that would be inactive toward Li intercalation (i.e. greatly increased the charge transfer resistance) but remain ineffective toward electrolyte degradation.

After the CC-CV cycling, the two main O 1s components of both the fresh graphite and NMC electrodes were replaced by two main peaks (Figures 4 and 5), in agreement with the formation of carbonaceous species from the solvents at the surface of both electrodes. The

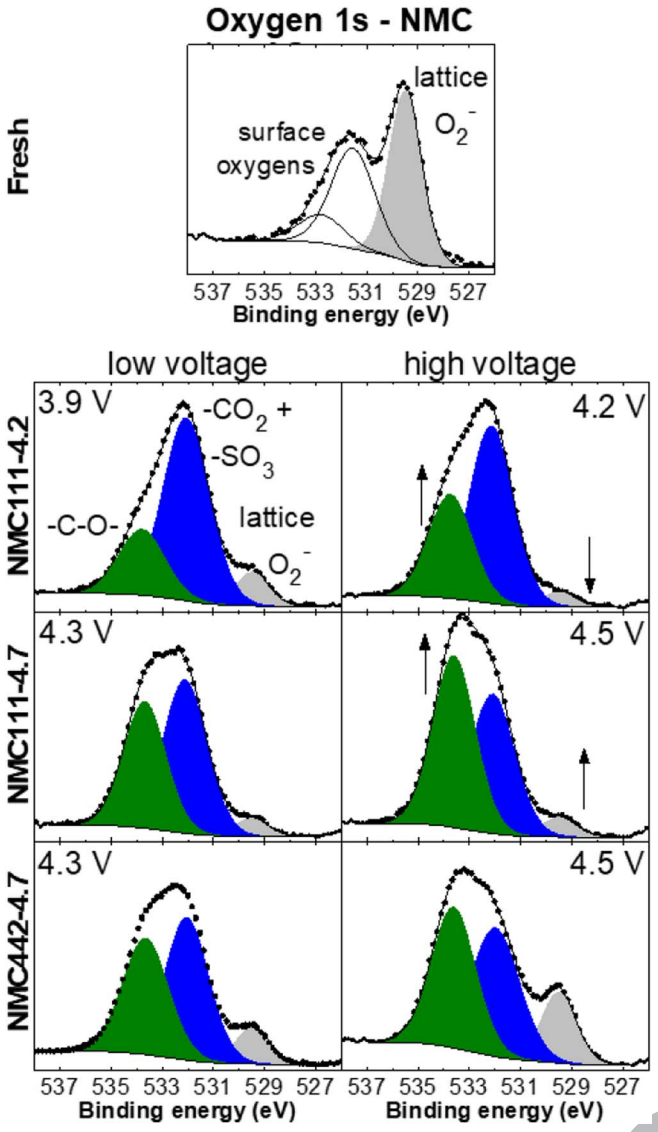

Figure 5. Oxygen 1s XPS core spectra of NMC electrodes as taken from the different NMC/graphite pouch cells after the CC-CV cycling procedure (i.e. 30 CC-CV cycles) at 2.8 V after discharge. ~~Typical Oxygen 1s XPS core spectra of fresh graphite and NMC electrodes are also showed for comparison.~~

peak at 533.8–533.5 eV is attributed to -CO bonds from $ROCO_2Li$ and/or ether derivatives.[76,77] The peak at 532–531.7 eV is assigned to -CO_2 oxygen from lithium alkyl carbonates ($ROCO_2Li$)[78,79] as well as to additional O contribution of sulfite species (RSO_3) from PES.[31,66] Additional weak peaks were also observed at ~530.7 and ~528.3 eV for the graphite electrodes, especially for low upper cutoff voltages, due to formation of lithium alkoxide (ROLi)[80,81] and lithium oxide (Li_2O)[82,83], respectively. As a whole, the chemical nature of the oxygen-containing compounds at both the graphite and NMC electrodes surface changes with the upper cutoff voltage. The ratio of oxygen in a -CO environment at 533.8–533.5 eV to a -CO_2 environment at 532–531.7 eV increased from 3.9 to 4.2 V and increased even more significantly from 4.3 to 4.5 V in good agreement with the increase of the carbon in a -CO environment at 286.9–287 eV (Figures 2 and 3). At this point, it has to be consider that: (i) this phenomenon is much more pronounced at the graphite electrodes surface while the graphite electrode potential is identical between low and high upper cutoff voltages; (ii) at 4.5 V, the SEI films thickness decreased at the NMC electrodes surface while the electrolyte degradation occurs at the NMC electrodes. Therefore, the additional -CO containing species has to be generated at the NMC electrodes surface then diffuse to the graphite electrodes where they are either reduced or simply deposited. At this point, it is reminded that such SEI films enrichment of -CO containing species already occurred between 3.9 and 4.2 V while less pronounced. It therefore indicates a similar reactivity between low and high voltages, which is here more likely catalyzed by the voltage increase. Note that it was also reported to be catalyzed by an increase of temperature.[36]

Fluorine 1s, Phosphorus 2 p and 75–40 eV region.—Figure 6 shows a) the Fluorine 1s, b) Phosphorus 2p and c) 75–40 eV XPS core spectra of graphite electrodes as taken from the different NMC/graphite pouch cells after the CC-CV cycling procedure (i.e. 30 CC-CV cycles) at 2.8 V after discharge. The F 1s spectra (Figure 6a) showed two peaks at about 685 and 687.1 eV due to the formation of LiF[38,77] as well as $Li_xPO_yF_z$[84] and/or remaining Li_xPF_y,[85] respectively. The P 2p spectra (Figure 6b) showed three components at 137.4, 134.8 and 133.5 eV attributed to $Li_xPO_yF_z$[72,38], Li_xPF_y[85] and phosphates (P_xO_y)[72,38], respectively. As a whole, when the upper cutoff voltage increased, higher LiF and phosphates/fluorophosphates contents were observed with, however, a more pronounced effect in the case of LiF in agreement with previous reports[66,86]. It is reminded that the potential of the graphite electrode is identical between the low and high upper cutoff voltages and that the electrolyte degradation occurs at the NMC electrodes. Therefore, at high voltage, the enrichment of LiF and P-based species of the graphite SEI films can have two explanations: (i) a higher reactivity of $LiPF_6$ at the NMC electrodes followed by the migration of the salt degradation products to the graphite electrode or (ii) a higher reactivity of $LiPF_6$ with solvent degradation products produced at the NMC electrodes. In that case, the reaction(s) between the solvent degradation products and $LiPF_6$ may occurred either at the NMC electrodes or at the graphite electrodes after their migration and/or after their migration and reduction. Finally, salts degradation products are either reduced or simply deposited at the graphite electrode.

The careful analysis of the 75–40 eV spectra of the graphite electrodes showed that only lithium (originated from SEI species) was detected for cells cycled at 3.9 and 4.2 V (Figure 6c). As soon as cells were cycled at 4.3 V, Mn was also detected followed by Ni and Co at 4.5 V due to the dissolution of the NMC material surface in good agreement with the literature.[60] Note, however, that the Mn, Ni and Co content at the graphite electrodes surface were below 1% each so that the dissolution of the NMC would rather be low. Note also that negligible amounts of LiF, Phosphate and fluorophosphates were also observed at the NMC electrodes surface after the CC-CV cycling with, however, no trend.

Sulfur 1s after CC-CV cycling.—Figure 7 shows the Sulfur 2p XPS core spectra of both a) graphite and b) NMC electrodes as taken from the different NMC/graphite pouch cells after the CC-CV cycling procedure (i.e. 30 CC-CV cycles) at 2.8 V after discharge. Depending on the potential, S 2p spectra of both graphite and NMC electrodes showed three components at 169.0–168.6, 167.0–166.5 eV and 163.8 eV assigned to organic sulfite species (RSO_3) such as RSO_3Li and/or $ROSO_2Li$,[87] inorganic Li_2SO_3,[87] as well as $RSSO_3$ such as $Li_2S_2O_3$[88] and/or -S- species[87] from the degradation of the PES additive, respectively. Importantly, for cells cycled to 3.9 V, only RSO_3Li and Li_2SO_3 was detected at the graphite electrodes surface while only RSO_3Li was observed at the NMC electrodes surface in agreement with our previous results[31,66]. For cells cycled to 4.2 V and higher voltage, however, RSO_3Li as well as reduced Li_2SO_3 and -S- species were observed at both graphite and NMC electrodes surfaces. Note that these additional sulfur species have never been observed using less aggressive cycling conditions[31,66] which emphasises the need of CC-CV procedure to greatly accelerate ageing phenomena. The appearance of these new sulfur species is assigned to further reaction of relatively unstable sulfite species formed initially. Most importantly, it is rather unexpected to observed the appearance of Li_2SO_3 and -S- species at the NMC electrodes surface while these species can only result from reduction.

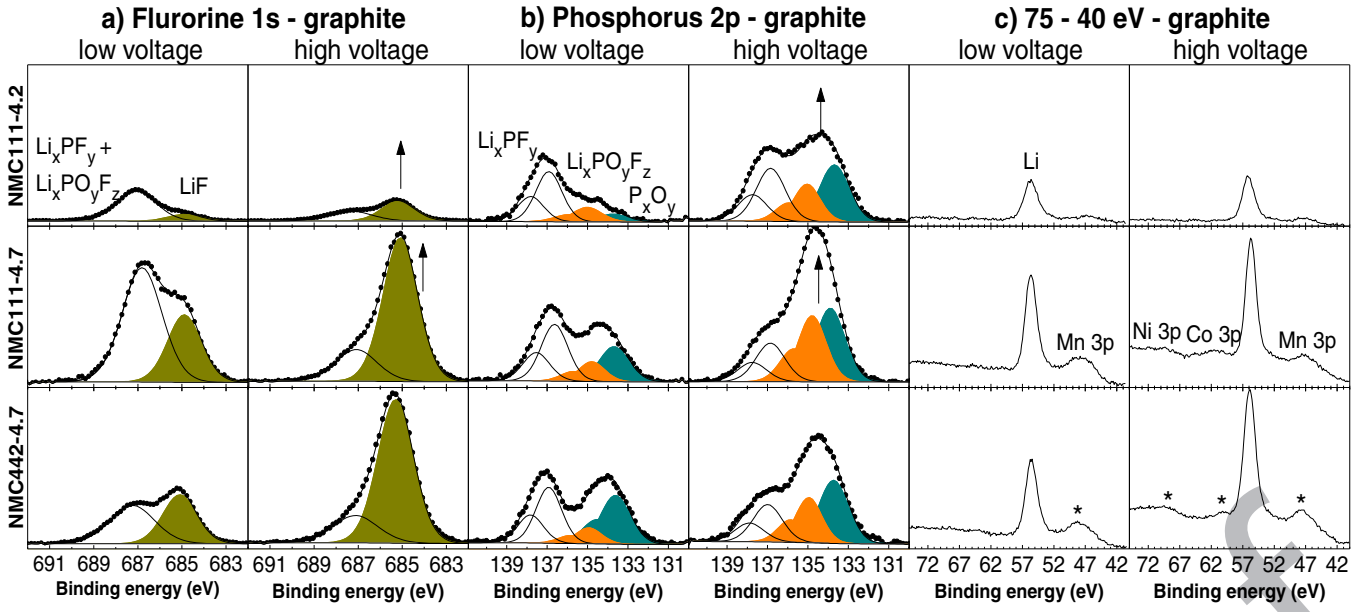

Figure 6. a) Fluorine 1s, b) Phosphorus 2p and c) 75–40 eV XPS core spectra of graphite electrodes as taken from the different NMC/graphite pouch cells after the CC-CV cycling procedure (i.e. 30 CC-CV cycles) at 2.8 V after discharge.

At first, it may appear that these reduced sulfur species are formed at the graphite electrodes then partially migrate to the NMC electrodes where they are deposited. However, as the graphite electrode potential is identical between low and high upper cutoff voltages, these reduced sulfur species would also be formed at 3.9 V which is not the case. Therefore, these reduced sulfur species might be formed somehow at the NMC electrodes surface by the electrons generated during oxidation processes. The exact phenomenon remains, however, unclear at this time. The large decrease of the total amount of sulfur species at the graphite electrodes surface between 4.3 and 4.5 V is explained by the large covering of the additional -CO containing species generated at the NMC electrodes at high voltage (Figures 4 and 5).

Conclusions

Interactions occurring between positive and negative electrodes during CC-CV cycling in Li[Ni$_{1/3}$Mn$_{1/3}$Co$_{1/3}$]O$_2$/graphite and Li[Ni$_{0.42}$Mn$_{0.42}$Co$_{0.16}$]O$_2$/graphite (NMC/graphite) pouch cells operating at different upper cutoff voltages have been thoroughly investigated. When cycled to 3.9, 4.2 and 4.3 V, NMC/graphite pouch cells showed good capacity retention, high and stable CE as well as low gas production while at 4.5 V, however, extensive capacity loss, dramatic and unstable CE as well as large gas generation were observed due to extensive electrolyte degradation at the NMC electrodes as soon as the cells are exposed for too much time at potentials above 4.3 V. XPS experiments showed that: (i) the thickness of the SEI films at

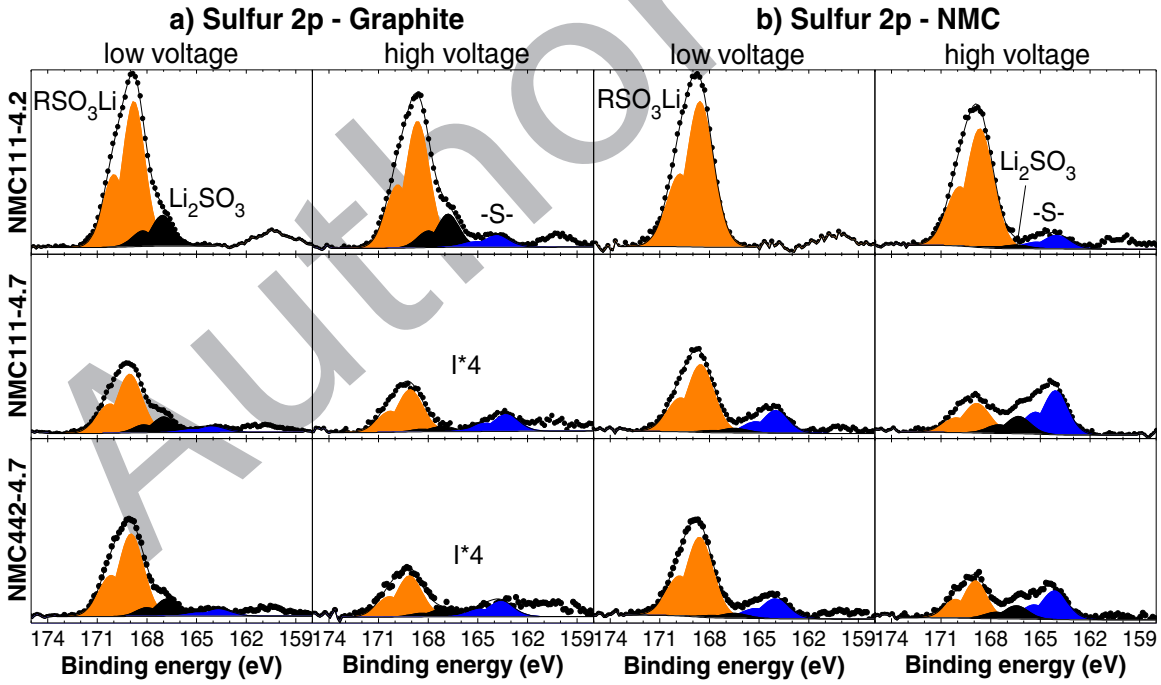

Figure 7. Sulfur 2p XPS core spectra of both a) graphite and b) NMC electrodes as taken from the different NMC/graphite pouch cells after the CC-CV cycling procedure (i.e. 30 CC-CV cycles) at 2.8 V after discharge.

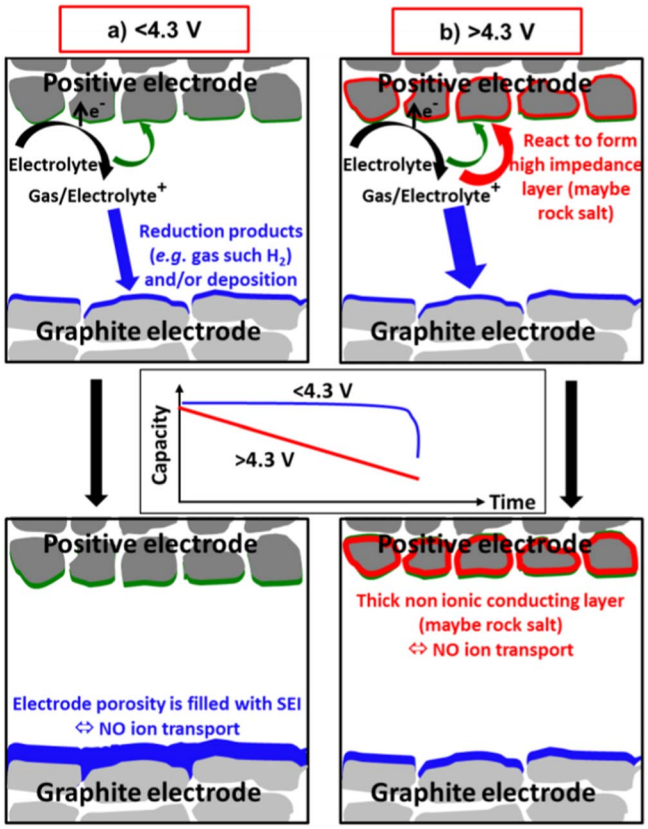

Figure 8. Schematic model of the two main failure mechanisms of Li-ion cells explained by interactions between positive and negative electrodes and corresponding capacity profile vs. time.

the NMC electrodes surface decreased between 4.3 and 4.5 V; (ii) an enrichment of -CO containing species occurred at the NMC electrodes surface and more importantly at the graphite electrodes surface as the cycling voltage increased, even between 3.9 and 4.2 V but especially at 4.5 V; (iii) an enrichment of LiF and P-based species occurred at the graphite electrodes surface as the cycling voltage increased; (iv) the successive appearance at the graphite electrodes surface of Mn then Ni and Co as soon as 4.3 V indicates the multistep dissolution of the NMC material at high voltage with, however, a limited extent; (v) additional reduced sulfur species were detected at both graphite and NMC electrodes surface as soon as cells were cycled to 4.2 V due to the further reaction of relatively unstable sulfite species. All these extensive parasitic reactions occurring at 4.5 V at the NMC electrodes lead to the formation of solvents and salt degradation products including gas as well as metallic species from the dissolution of NMC that migrate to the graphite electrodes surface where they are either reduced or simply deposited.

Considering the literature reports and experimental results discussed here, two main failure mechanism of Li-ion cells during cycling are proposed as illustrated in Figure 8. First, at low voltage (i.e. <4.3 V, Figure 8a), electrolyte degradation products are created at the positive electrode with at a relatively slow rate then migrate to the negative electrode where they are either reduced and/or deposited which implies that the graphite SEI film is not electronically insulating. After sufficient time, the accumulation of unwanted solid products at the graphite electrode surface results in the large hindrance of the electrode porosity (i.e. the ionic transport) and concomitant rapid capacity rollover[58,89]. Note that if the loss of active lithium inventory and/or large impedance increase occur at low voltage, a common gradual capacity loss will occur before the cell can suffer from the rapid rollover effect. Second, at high voltage (>4.3 V, Figure 8b), extensive electrolyte degradation products are created at the positive electrode at a relatively high rate then migrate to the negative electrode where they are either reduced and/or deposited. However, the dramatic charge transfer resistance increase (i.e. kinetic hindrance) at the NMC particles surface is the dominant failure mechanism at high voltage an occur through the formation of a surface layer (maybe rock salt) inactive toward Li intercalation (Li-ion insulator) but ineffective toward electrolyte degradation (electron conductor) due to irreversible structural change of the NMC particles surface during cycling. Overall, both failure mechanisms are driven by oxidative parasitic reactions at the positive electrode surface which means that the passivation of the positive electrode would be the key for long lifetime of Li-ion cells.

Finally, this study clearly demonstrated that a better understanding of the interactions occurring between the positive and negative electrodes and their impacts on the SEI films formation and evolution is a crucial point if one want to further optimize cell performance, lifetime and safety of Li-ion cells, especially at high voltage. To do so, however, the study of half cells with lithium as negative electrode should necessarily be coupled to full cell investigation if relevant results want to be gathered. Last but not least, aggressive CC-CV cycling should also be preferred to accelerate ageing phenomena compared to the commonly used CC cycling that mislead the reality of commercial cells use especially at high rate.

References

1. D. Andre, S. -J. Kim, P. Lamp, S. F. Lux, F. Maglia, O. Paschos, and B. Stiaszny, *J. Mater. Chem. A*, **3**, 6709 (2015).
2. W. Huang, L. Xing, Y. Wang, M. Xu, W. Li, F. Xie, and S. Xia, *J. Power Sources*, **267**, 560 (2014).
3. L. Xia, Y. Xia, and Z. Liu, *Electrochim. Acta*, **151**, 429 (2015).
4. J. Xia, M. Nie, L. Ma, and J. R. Dahn, *J. Power Sources*, **306**, 233 (2016).
5. S. S. Zhang, *J. Power Sources*, **162**, 1379 (2006).
6. K. Xu, *Chem. Rev.*, **114**, 11503 (2014).
7. E. Peled, *J. Electrochem. Soc.*, **126**, 2047 (1979).
8. B. Simon and J.-P. Boeuve, Rechargeable Lithium Electrochemical Cell. U.S. Pat. 5,626,981, 1997.
9. M. Contestabile, M. Morselli, R. Paraventi, and R. J. Neat, *J. Power Sources*, **119–121**, 943 (2003).
10. M. Holzapfel, C. Jost, A. Prodi-Schwab, F. Krumeich, A. Würsig, H. Buqa, and P. Novák, *Carbon N. Y.*, **43**, 1488 (2005).
11. T. Sasaki, T. Abe, Y. Iriyama, M. Inaba, and Z. Ogumi, *J. Electrochem. Soc.*, **152**, A2046 (2005).
12. E. G. Shim, T. H. Nam, J. G. Kim, H. S. Kim, and S. I. Moon, *J. Power Sources*, **172**, 901 (2007).
13. L. Chen, K. Wang, X. Xie, and J. Xie, *J. Power Sources*, **174**, 538 (2007).
14. N. N. Sinha, A. J. Smith, J. C. Burns, G. Jain, K. W. Eberman, E. Scott, J. P. Gardner, and J. R. Dahn, *J. Electrochem. Soc.*, **158**, A1194 (2011).
15. J. C. Burns, G. Jain, A., J. Smith, K. W. Eberman, E. Scott, J. P. Gardner, and J. R. Dahn, *J. Electrochem. Soc.*, **158**, A255 (2011).
16. J. Jeon, S. Yoon, T. Park, J. -J. Cho, S. Kang, Y. -K. Han, and H. Lee, *J. Mater. Chem.*, **22**, 21003 (2012).
17. H. M. Jung, S. -H. Park, J. Jeon, Y. Choi, S. Yoon, J. -J. Cho, S. Oh, S. Kang, Y. -K. Han, and H. Lee, *J. Mater. Chem. A*, **1**, 11975 (2013).
18. X. Zuo, C. Fan, X. Xiao, J. Liu, and J. Nan, *J. Power Sources*, **219**, 94 (2012).
19. X. Zuo, C. Fan, X. Xiao, J. Liu, and J. Nan, *ECS Electrochem. Lett.*, **1**, A50 (2012).
20. X. Zuo, J. Wu, C. Fan, K. Lai, J. Liu, and J. Nan, *Electrochim. Acta*, **130**, 778 (2014).
21. T. Huang, M. Wu, W. Wang, Y. Pan, and G. Fang, *J. Power Sources*, **262**, 303 (2014).
22. F. Bian, Z. Zhang, and Y. Yang, *J. Energy Chem.*, **23**, 383 (2014).
23. J. Xia, N. N. Sinha, L. P. Chen, G. Y. Kim, D. J. Xiong, and J. R. Dahn, *J. Electrochem. Soc.*, **161**, A84 (2014).
24. J. Xia, N. N. Sinha, L. P. Chen, and J. R. Dahn, *J. Electrochem. Soc.*, **161**, A264 (2014).
25. B. Li, M. Xu, T. Li, W. Li, and S. Hu, *Electrochem. commun.*, **17**, 92 (2012).
26. B. Li, M. Xu, B. Li, Y. Liu, L. Yang, W. Li, and S. Hu, *Electrochim. Acta*, **105**, 1 (2013).
27. B. Li, Y. Wang, W. Tu, Z. Wang, M. Xu, L. Xing, and W. Li, *Electrochim. Acta*, **147**, 636 (2014).
28. B. Li, Y. Q. Wang, H. B. Rong, Y. T. Wang, J. S. Liu, L. D. Xing, M. Q. Xu, and W. S. Li, *J. Mater. Chem. A*, **1**, 12954 (2013).
29. J. Xia, L. Ma, C. P. Aiken, K. J. Nelson, L. P. Chen, and J. R. Dahn, *J. Electrochem. Soc.*, **161**, A1634 (2014).
30. K. J. Nelson, J. Xia, and J. R. Dahn, *J. Electrochem. Soc.*, **161**, A1884 (2014).
31. L. Madec, R. Petibon, J. Xia, J. -P. Sun, I. G. Hill, and J. R. Dahn, *J. Electrochem. Soc.*, **162**, A2635 (2015).
32. J. Self, D. S. Hall, L. Madec, and J. R. Dahn, *J. Power Sources*, **298**, 369 (2015).
33. J. Xia, K. J. Nelson, Z. Lu, and J. R. Dahn, *J. Power Sources*, **329**, 387 (2016).
34. K. J. Nelson, D. W. Abarbanel, J. Xia, Z. Lu, and J. R. Dahn, *J. Electrochem. Soc.*, **163**, A272 (2016).

35. E. Markevich, G. Salitra, K. Fridman, R. Sharabi, G. Gershinsky, A. Garsuch, G. Semrau, M. A. Schmidt, and D. Aurbach, *Langmuir*, **30**, 7414 (2014).
36. D. Lu, M. Xu, L. Zhou, A. Garsuch, and B. L. Lucht, *J. Electrochem. Soc.*, **160**, A3138 (2013).
37. L. Yang, B. Ravdel, and B. L. Lucht, *Electrochem. Solid-State Lett.*, **13**, A95 (2010).
38. H. Bouayad, Z. Wang, N. Dupré, R. Dedryvère, D. Foix, S. Franger, J. F. Martin, L. Boutafa, S. Patoux, D. Gonbeau, and D. Guyomard, *J. Phys. Chem. C*, **118**, 4634 (2014).
39. X. Li, M. Xu, Y. Chen, and B. L. Lucht, *J. Power Sources*, **248**, 1077 (2014).
40. P. Yang, J. Zheng, S. Kuppan, Q. Li, D. Lv, J. Xiao, G. Chen, J. G. Zhang, and C. M. Wang, *Chem. Mater.*, **27**, 7447 (2015).
41. R. Wagner, M. Korth, B. Streipert, J. Kasnatscheew, D. R. Gallus, S. Brox, M. Amereller, I. Cekic-Laskovic, and M. Winter, *ACS Appl. Mater. Interfaces*, **8**, 30871 (2016).
42. C. H. Chen, J. Liu, and K. Amine, *J. Power Sources*, **96**, 321 (2001).
43. R. Petibon, C. P. P. Aiken, N. N. N. Sinha, J. C. C. Burns, H. Ye, C. M. VanElzen, G. Jain, S. Trussler, and J. R. R. Dahn, *J. Electrochem. Soc.*, **160**, A117 (2013).
44. Y. Zhang and C. -Y. Wang, *J. Electrochem. Soc.*, **156**, A527 (2009).
45. D. W. Abarbanel, K. J. Nelson, and J. R. Dahn, *J. Electrochem. Soc.*, **163**, A522 (2016).
46. S. Muto, Y. Sasano, K. Tatsumi, T. Sasaki, K. Horibuchi, Y. Takeuchi, and Y. Ukyo, *J. Electrochem. Soc.*, **156**, A371 (2009).
47. S. Zheng, R. Huang, Y. Makimura, Y. Ukyo, C. a., J. Fisher, T. Hirayama, and Y. Ikuhara, *J. Electrochem. Soc.*, **158**, A357 (2011).
48. F. Lin, I. M. Markus, D. Nordlund, T. -C. Weng, M. D. Asta, H. L. Xin, and M. M. Doeff, *Nat. Commun.*, **5**, 3529 (2014).
49. I. Buchberger, S. Seidlmayer, A. Pokharel, M. Piana, J. Hattendorff, P. Kudejova, R. Gilles, and H. A. Gasteiger, *J. Electrochem. Soc.*, **162**, 2737 (2015).
50. X. Li, Y. Chen, C. C. Nguyen, M. Nie, and B. L. Lucht, *J. Electrochem. Soc.*, **161**, A576 (2014).
51. R. Younesi, A. S. Christiansen, R. Scipioni, D. -T. Ngo, S. B. Simonsen, K. Edström, J. Hjelm, and P. Norby, *J. Electrochem. Soc.*, **162**, A1289 (2015).
52. M. Metzger, C. Marino, J. Sicklinger, D. Haering, and H. A. Gasteiger, *J. Electrochem. Soc.*, **162**, A1123 (2015).
53. M. Metzger, J. Sicklinger, D. Haering, C. Kavakli, C. Stinner, C. Marino, and H. A. Gasteiger, *J. Electrochem. Soc.*, **162**, A1227 (2015).
54. X. Qi, B. Blizanac, A. DuPasquier, A. Lal, P. Niehoff, T. Placke, M. Oljaca, J. Li, and M. Winter, *J. Electrochem. Soc.*, **162**, A339 (2015).
55. R. Spotnitz, *J. Power Sources*, **113**, 72 (2003).
56. S. E. Sloop, J. B. Kerr, and K. Kinoshita, *J. Power Sources*, **119–121**, 330 (2003).
57. R. Dedryveère, D. Foix, S. Franger, S. Patoux, L. Daniel, and D. Gonbeau, *J. Phys. Chem. C*, **114**, 10999 (2010).
58. J. C. Burns, A. Kassam, N. N. Sinha, L. E. Downie, L. Solnickova, B. M. Way, and J. R. Dahn, *J. Electrochem. Soc.*, **160**, A1451 (2013).
59. Y. Talyosef, B. Markovsky, G. Salitra, D. Aurbach, H. Kim, and S. Choi, *J. Power Sources*, **146**, 664 (2005).
60. H. Zheng, Q. Sun, G. Liu, X. Song, and V. S. Battaglia, *J. Power Sources*, **207**, 134 (2012).
61. M. Metzger, B. Strehle, S. Solchenbach, and H. A. Gasteiger, *J. Electrochem. Soc.*, **163**, A798 (2016).
62. D. J. Xiong, L. D. Ellis, R. Petibon, T. Hynes, Q. Q. Liu, and J. R. Dahn, **164**, 1 (2017).
63. D. J. Xiong, R. Petibon, M. Nie, L. Ma, J. Xia, and J. R. Dahn, *J. Electrochem. Soc.*, **163**, A546 (2016).
64. R. Petibon, L. Madec, L. M. Rotermund, and J. R. Dahn, *J. Power Sources*, **313**, 152 (2016).
65. H. M. Dahn, a., J. Smith, J. C. Burns, D. A. Stevens, and J. R. Dahn, *J. Electrochem. Soc.*, **159**, A1405 (2012).
66. L. Madec, L. Ma, K. J. Nelson, R. Petibon, J. -P. Sun, I. G. Hill, and J. R. Dahn, *J. Electrochem. Soc.*, **163**, A1001 (2016).
67. J. Self, C. P. Aiken, R. Petibon, and J. R. Dahn, *J. Electrochem. Soc.*, **162**, A796 (2015).
68. C. P. Aiken, J. Xia, D. Y. Wang, D. A. Stevens, S. Trussler, and J. R. Dahn, *J. Electrochem. Soc.*, **161**, A1548 (2014).
69. L. Madec, J. Xia, R. Petibon, K. J. Nelson, J. -P. Sun, I. G. Hill, and J. R. Dahn, *J. Phys. Chem. C*, **118**, 29608 (2014).
70. D. A. Shirley, *Phys. Rev. B*, **5**, 4709 (1972).
71. K. J. Nelson, G. L. D 'eon, A. T. B. Wright, L. Ma, J. Xia, and J. R. Dahn, *J. Electrochem. Soc.*, **162**, 1046 (2015).
72. L. El Ouatani, R. Dedryvère, C. Siret, P. Biensan, S. Reynaud, P. Iratçabal, and D. Gonbeau, *J. Electrochem. Soc.*, **156**, A103 (2009).
73. D. Pantea, H. Darmstadt, S. Kaliaguine, L. Sümmchen, and C. Roy, *Carbon N. Y.*, **39**, 1147 (2001).
74. D. Pantea, H. Darmstadt, S. Kaliaguine, and C. Roy, *Appl. Surf. Sci.*, **217**, 181 (2003).
75. W. Li, A. Dolocan, P. Oh, H. Celio, S. Park, J. Cho, and A. Manthiram, *Nat. Commun.*, **8**, 14589 (2017).
76. R. Dedryvère, L. Gireaud, S. Grugeon, S. Laruelle, J. M. Tarascon, and D. Gonbeau, *J. Phys. Chem. B*, **109**, 15868 (2005).
77. S. Malmgren, K. Ciosek, M. Hahlin, T. Gustafsson, M. Gorgoi, H. Rensmo, and K. Edström, *Electrochim. Acta*, **97**, 23 (2013).
78. D. Aurbach, M. L. Daroux, P. W. Faguy, and E. Yeager, *J. Electrochem. Soc.*, **134**, 1611 (1987).
79. M. Nie, D. Chalasani, D. P. Abraham, Y. Chen, A. Bose, and B. L. Lucht, *J. Phys. Chem. C*, **117**, 1257 (2013).
80. M. Onuki, S. Kinoshita, Y. Sakata, M. Yanagidate, Y. Otake, M. Ue, and M. Deguchi, *J. Electrochem. Soc.*, **155**, A794 (2008).
81. R. Petibon, L. M. Rotermund, and J. R. Dahn, *J. Power Sources*, **287**, 184 (2015).
82. I. Ismail, A. Noda, A. Nishimoto, and M. Watanabe, *Electrochim. Acta*, **46**, 1595 (2001).
83. L. J. Rendek, G. S. Chottiner, and D. A. Scherson, *J. Electrochem. Soc.*, **149**, E408 (2002).
84. B. Ravdel, K. M. Abraham, R. Gitzendanner, J. DiCarlo, B. Lucht, and C. Campion, *J. Power Sources*, **119–121**, 805 (2003).
85. K. Edström, T. Gustafsson, and J. O. Thomas, *Electrochim. Acta*, **50**, 397 (2004).
86. R. Dedryvère, H. Martinez, S. Leroy, D. Lemordant, F. Bonhomme, P. Biensan, and D. Gonbeau, *J. Power Sources*, **174**, 462 (2007).
87. H. Ota, T. Akai, H. Namita, S. Yamaguchi, and M. Nomura, *J. Power Sources*, **119–121**, 567 (2003).
88. S. Xiong, K. Xie, Y. Diao, and X. Hong, *J. Power Sources*, **246**, 840 (2014).
89. L. Boulet-Roblin, M. E. Kazzi, P. Novak, and C. Villevieille, *J. Electrochem. Soc.*, **162**, A1297 (2015).

Queries

Q1: AU: Please provide a digital object identifier (doi) for Ref(s) 48, and 62. For additional information on doi's please select this link: http://www.doi.org/. If a doi is not available, no other information is needed from you.

Q2: AU: Please provide complete details of ref. 62.